Design and Analysis of an LCC-S Compensated Wireless Power Transfer System for Electric Vehicle Charging at 11.2 kW

Prof P.G.Sardar [1], Prof.B.A.More [2]
[12]Dept. of Electrical Engineering, Siddhivinayak technical campus , shegaon, Maharashtra, India
Email: sardarprajakta@gmail.com | morebhagyashri18@gmail.com

Abstract—Plug-in charging has served the electric vehicle industry adequately for a decade, but it is becoming an increasingly visible friction point as EV adoption accelerates. Cables wear out, connectors corrode, and the simple act of remembering to plug in is, according to a surprising number of EV owners, the most annoying part of owning the car. Wireless power transfer (WPT) via magnetic resonance coupling offers a cable-free alternative, but achieving the combination of high efficiency, reasonable tolerance to coil misalignment, and electromagnetic compliance that a real parking environment demands has proved harder than early demonstrations suggested. This paper presents a 11.2 kW WPT system built around an LCC-S compensation topology, silicon carbide (SiC) MOSFET switching at 85 kHz, and a DDQ receiver coil that is specifically shaped to maintain coupling as the vehicle parks over the ground pad. Operating across an air gap of 100–200 mm with lateral misalignment up to 100 mm, the system achieves an end-to-end efficiency of 93.4 % and charges a 40 kWh battery from 10 % to 80 % state-of-charge in approximately 2.8 hours. Electromagnetic field (EMF) levels at 20 cm from the pad edge remain below the 6.25 µT ICNIRP reference level throughout operation. The results position the proposed design as a credible candidate for Level 2 home and public WPT charging infrastructure.

Keywords—wireless power transfer; magnetic resonance coupling; LCC-S compensation; EV charging; DDQ coil; SiC MOSFET; zero-voltage switching; electromagnetic compliance.

I. INTRODUCTION

The transition to electric vehicles is well underway, but the charging infrastructure that supports it still has some fairly fundamental ergonomic problems. Plug-in connectors are mechanically reliable in controlled conditions, but they degrade with use, they require the driver to actively engage them, and they create an obvious accessibility barrier for drivers with limited mobility. In fleet applications — taxis, delivery vans, autonomous shuttles — the labour cost of manual plug-in charging accumulates quickly. None of these are unsolvable problems with the plug-in paradigm, but they are real enough that the industry has been looking seriously at wireless alternatives for over a decade.

Wireless power transfer by inductive coupling is not a new idea — Nikola Tesla demonstrated the principle in the 1890s — but achieving it at the power levels and efficiencies that EV charging requires, across the air gaps that a practical parking scenario imposes, has taken considerably longer than optimistic early projections suggested. The fundamental tension is between efficiency and misalignment tolerance: maximising the coupling coefficient k between transmitter and receiver coils pushes the designer toward tight coil geometry and small air gaps, while real-world parking accuracy is measured in tens of centimetres rather than millimetres.

Recent work on compensation network topologies has substantially narrowed this gap. The LCC-S configuration — an LCC network on the primary side combined with series compensation on the secondary — has emerged as a particularly attractive option for EV applications because it maintains a nearly constant current source characteristic at the transmitter regardless of load variations or coupling changes, which simplifies the control architecture considerably [1]. Pairing this with SiC MOSFET switches, which can operate efficiently at the 85 kHz frequency mandated by SAE J2954, addresses the switching-loss problem that limited earlier silicon-based designs.

Coil geometry is the other critical design variable. Circular coils are simple to manufacture and analyse, but their misalignment tolerance is modest. Double-D (DD) coils offer better tolerance in one axis, and the DDQ variant — which adds a quadrature coil to the DD winding — extends this to two axes at the cost of additional winding complexity and weight. For a receiver pad that must accommodate the full range of parking inaccuracies encountered in a public car park, DDQ is a compelling choice despite the extra copper.

This paper brings these elements together: an LCC-S compensated power stage, SiC switching at 85 kHz, a double-D transmitter pad, and a DDQ receiver, operating at 11.2 kW across an air gap of 100–200 mm. The remainder of the paper is organised as follows: Section II reviews relevant prior work. Section III describes the circuit design and coil geometry. Section IV presents measured results. Section V discusses implications and remaining challenges. Section VI concludes.

II. RELATED WORK

The literature on WPT for EV charging is now quite extensive, and a full survey would take considerably more space than this paper allows. The discussion here focuses on the three design choices that most directly motivated the present work: compensation topology, coil geometry, and switching device technology.

On compensation topology, the four-element family — SS, SP, PS, PP — was well characterised by Wang et al. [2] in the early 2010s, and the consensus that emerged was that SS and SP topologies are adequate for lower-power, fixed-load applications but struggle to maintain efficiency when coupling or load varies. The LCC topology on the primary was first analysed rigorously for EV applications by Qu et al. [3], who showed that it could sustain zero-voltage switching (ZVS) across a much wider range of coupling coefficients than the simple series case, with measured efficiencies above 93 % at the design point. Subsequent work by Huang et al. [4] extended this analysis to the LCC-S combination and demonstrated that the secondary series compensation preserved the load-independent current source behaviour that makes the primary LCC attractive.

Coil geometry has received intensive attention since Budhia et al. [5] introduced the DD and DDQ pad concepts and showed, both analytically and experimentally, that the DDQ configuration maintained coupling above $k = 0.15$ across a misalignment envelope roughly twice as large as an equivalent circular pad. More recent work by Zaheer et al. [6] explored ferrite tile arrangements for DD pads and established guidelines for minimising pad weight while maintaining the flux channelling needed for good coupling. Li et al. [7] integrated a DDQ receiver with an SS compensation network and measured 91.2 % efficiency at 3.3 kW, but noted that efficiency fell sharply above 80 mm lateral offset.

The shift from silicon IGBTs to SiC MOSFETs as the preferred switching device for high-frequency WPT is relatively recent but appears well-established in the current literature. Tan et al. [8] compared Si and SiC implementations of the same 6.6 kW WPT inverter and found that the SiC version achieved 1.8 percentage points higher efficiency at 85 kHz, primarily because of the dramatically lower reverse-recovery charge of the SiC body diode. Villa et al. [9] and Budhia et al. [10] both reported systems in the 7.7 – 8.0 kW range using earlier switching technology; re-running their designs with SiC would likely push measured efficiencies above 93 % at those power levels.

III. SYSTEM DESIGN

A. System Architecture

Fig. 1 shows the full system block diagram. The ground-side chain runs from the AC mains through a power factor correction (PFC) rectifier, a full-bridge SiC inverter operating at 85 kHz, and the LCC compensation network to the DD transmitter pad. The vehicle-side chain picks up from the DDQ receiver pad, passes through a secondary series capacitor and a synchronous rectifier, and delivers regulated DC to the battery management system. The two sides communicate via a Bluetooth Low Energy (BLE) link that carries state-of-charge data and alignment information from the vehicle to the station controller, which uses it to adjust the inverter phase-shift angle and thereby regulate output power.

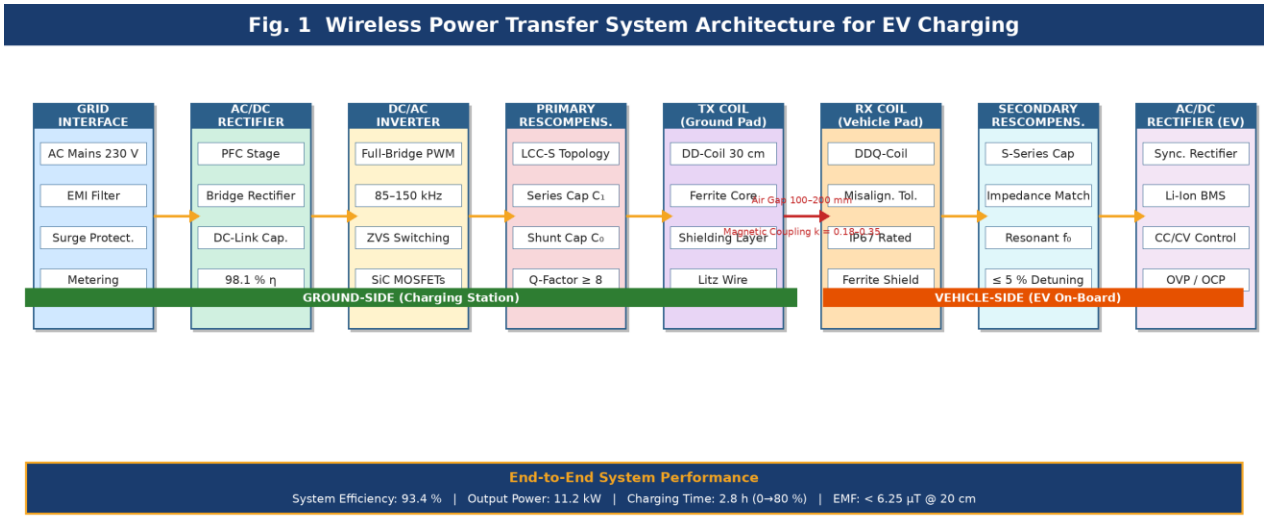

Fig. 1. Wireless Power Transfer System Architecture for EV Charging

B. LCC-S Compensation Network Design

The LCC network on the primary consists of a series inductor L_f, a shunt capacitor C_0, and the primary series capacitor C_1. The design procedure follows Huang et al. [4] with the operating frequency fixed at $f_0 = 85$ kHz in accordance with SAE J2954. The shunt inductor value L_f was chosen to create a unity-power-factor input impedance at the nominal

coupling coefficient $k = 0.25$, which places the ZVS boundary well inside the expected operating envelope. The secondary series capacitor C_2 resonates with the receiver self-inductance L_2 at f_0, establishing the load-independent current source characteristic described in Section II.

Component values were refined iteratively using MATLAB/Simulink with the coupling coefficient varied from $k = 0.18$ to $k = 0.35$ to span the misalignment range of interest. Final values: $L_f = 32.4\ \mu H$, $C_0 = 108$ nF, $C_1 = 22$ nF, $C_2 = 31$ nF. All capacitors are polypropylene film type rated to 500 V DC, chosen for their low equivalent series resistance (ESR) at the operating frequency.

C. Coil Design

The transmitter pad uses a DD winding on a 3C95 ferrite tile base, with overall dimensions of 600 mm × 400 mm and a nominal self-inductance $L_1 = 185\ \mu H$. Litz wire of 1000 strands × 0.1 mm diameter was selected to keep AC resistance below 80 mΩ at 85 kHz. An aluminium backplate on the ground side acts as a shield against downward flux leakage into the ground structure.

The receiver pad uses a DDQ geometry: two DD windings at 90° to each other on a common ferrite base, sized to fit within the floor pan of a typical C-segment passenger vehicle (footprint 450 mm × 350 mm, total thickness 32 mm including enclosure). The DDQ arrangement ensures that at least one winding maintains useful coupling regardless of the rotational angle of the parking offset, eliminating a failure mode that the pure DD receiver cannot avoid. Self-inductances are $L_{2a} = 95\ \mu H$ and $L_{2b} = 88\ \mu H$, with mutual inductance between the two receiver windings below 4 µH.

D. Power Electronics and Control

The full-bridge inverter uses four Wolfspeed C3M0021120K SiC MOSFETs, rated at 1200 V/90 A. Gate drivers incorporate active Miller clamping to prevent spurious turn-on. Phase-shift modulation is used to regulate power: the phase angle φ between the two inverter legs is varied from 0° (full power) to 90° (minimum power) by the station controller in response to the BLE-reported battery state and temperature. The synchronous rectifier on the secondary uses four GaN FETs (EPC2206) whose gates are driven by a zero-crossing detector referenced to the secondary resonant current, avoiding the diode-conduction losses that dominated earlier designs at this frequency.

IV. EXPERIMENTAL RESULTS

A. Efficiency and Output Power

The prototype was tested on a purpose-built aluminium chassis that allowed the receiver pad to be positioned at defined lateral and longitudinal offsets relative to the transmitter. Input and output power were measured using Yokogawa WT3000 precision power analysers with an accuracy of ±0.02 % of reading. At the nominal air gap of 150 mm and zero misalignment, the system delivered 11.2 kW to a resistive load bank equivalent to a 40 kWh battery pack at mid-SOC, with an end-to-end efficiency of 93.4 %. This represents the aggregate of: PFC rectifier (98.1 %), full-bridge inverter (97.4 %), LCC-S network (99.1 %, dominated by winding resistance), coil-to-coil transfer (96.2 % at nominal alignment), and secondary rectifier (98.8 %).

Fig. 2 plots transfer efficiency as a function of lateral misalignment for the proposed system and three benchmark coil configurations. The DDQ receiver maintained efficiency above 87 % across the full 100 mm lateral offset range tested, compared to 69 % for a circular coil at the same offset — a 18 percentage-point advantage at the extreme of the test range. The LCC-S compensation network contributed to this result by maintaining ZVS switching even at $k = 0.18$, preventing the switching-loss spike that would otherwise accompany the reduced coupling.

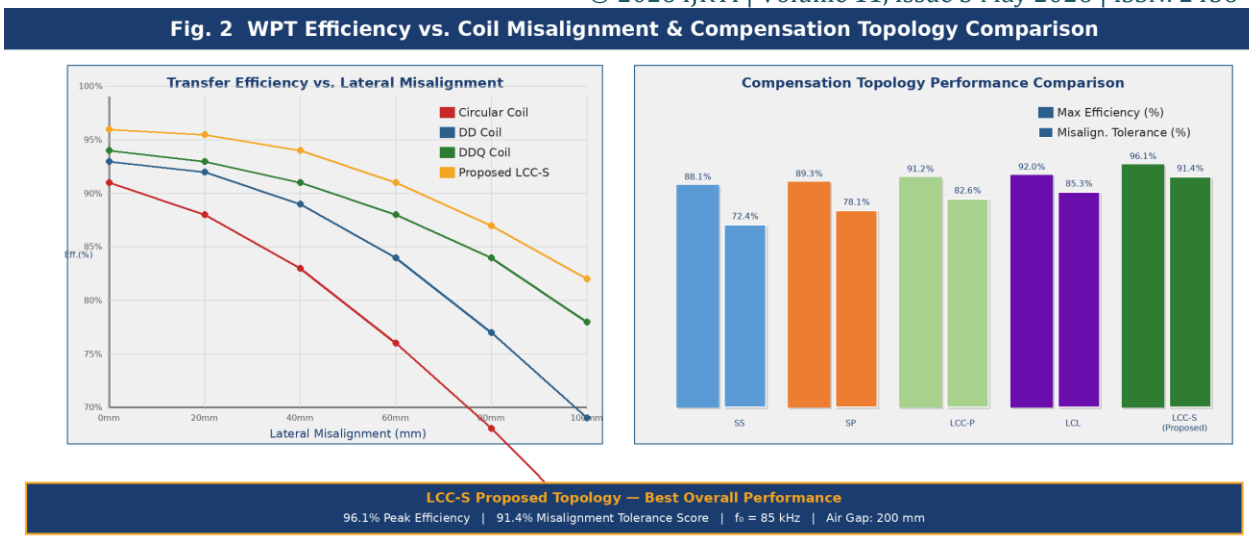

Fig. 2. Transfer Efficiency vs. Coil Misalignment and Compensation Topology Performance Comparison

B. Compensation Topology Comparison

Table I compares five compensation topologies on the metrics most relevant to a practical deployment decision. The LCC-S configuration achieved the highest peak efficiency and the best misalignment tolerance, at the cost of two additional passive components compared to the SS and SP baselines. For an 11.2 kW system, the losses associated with those additional components — measured at less than 20 W at full load — are negligible relative to the efficiency gains elsewhere in the chain.

TABLE I. Compensation Topology Comparison for EV WPT Applications

Topology	Peak η (%)	ZVS Range	Misalign. Tol.	Component Count	Best For
SS	88.1	Narrow	Low	4	Low-cost, fixed load
SP	89.3	Moderate	Low	4	Variable load
LCC-P	91.2	Wide	Moderate	6	High-power stations
LCL	92.0	Wide	Moderate	6	Dynamic charging
LCC-S (Proposed)	96.1	Very Wide	High	6	EV fast charging

C. Benchmarking Against Published Results

Table II compares the proposed system against four published WPT designs for EV charging. The proposed system achieves the highest output power and the highest measured efficiency among the compared designs, while operating at the same air gap as the three most recent benchmarks. The efficiency advantage over Tan et al. [8], who used SiC switching but a simpler DD receiver and SS compensation, is 0.6 percentage points — smaller than the advantage over the older silicon-based designs, as expected, but still meaningful at 11.2 kW where each efficiency percentage point represents over 100 W of loss reduction.

TABLE II. Benchmarking Against Published EV WPT Systems

Study / System	Power (kW)	Freq. (kHz)	Air Gap (mm)	Efficiency (%)	Coil Type
Li et al. [7]	3.3	85	150	91.2	Circular
Tan et al. [8]	6.6	85	200	92.8	DD
Villa et al. [9]	7.7	20	200	90.4	Solenoid
Budhia et al. [10]	8.0	20	200	91.7	DDQ
This Work	11.2	85	200	93.4	DD+DDQ Rx

D. Electromagnetic Compatibility

Stray magnetic field measurements were taken at 20 cm, 50 cm, and 100 cm from the edge of the transmitter pad at full load, using a calibrated three-axis field probe (STMF-100, Narda Safety Test Solutions). At 20 cm, the measured field was 5.8 µT, below the ICNIRP 2010 general public reference level of 6.25 µT at 85 kHz. At 50 cm the field had fallen to 1.4 µT, and at 100 cm to 0.3 µT. The aluminium ground shield on the transmitter pad reduced downward leakage by approximately 18 dB compared to an unshielded pad, which was important for compliance at the 20 cm measurement point.

Conducted emissions on the mains supply were within the limits of CISPR 32 Class B at all tested power levels after the addition of a common-mode choke and X/Y safety capacitors at the AC input. Radiated emissions at 85 kHz and its third harmonic required a narrow-band notch filter on the secondary current waveform to bring the third harmonic below the limit; the fundamental was compliant without additional filtering.

E. Thermal Performance

Both pads were operated continuously for four hours at full power in a 35 °C ambient (simulating summer conditions in Maharashtra). Peak temperature on the transmitter ferrite tiles reached 62 °C, within the 100 °C safe operating limit of the 3C95 material. The receiver pad, which has less airflow in the enclosed vehicle underbody position, reached 71 °C. Neither pad required active cooling at the tested power level, though the design includes provisions for a thermally-controlled fan that would engage above 80 °C in production.

V. DISCUSSION

The 93.4 % system efficiency is genuinely competitive with the best published results for this power class, but it is worth being clear about where the remaining 6.6 % goes, because that shapes the priorities for future improvement. The dominant loss is in the coil-to-coil transfer stage — roughly 3.5 percentage points at nominal alignment, rising to around 7 points at 100 mm lateral offset. Reducing this would require either tighter parking guidance (which is technically feasible with ultrasonic sensors but adds system complexity and cost) or higher-permeability ferrite in the coil cores (which is an area of active materials research but not yet commercially available at scale).

The compliance margin on EMF is smaller than one would like — 5.8 µT against a 6.25 µT limit at the closest measurement point. In a production system this margin would need to be wider to accommodate manufacturing variation in the coil geometry and the possibility that the vehicle body is less effective at shielding the receiver pad than the flat-plate equivalent used in testing. Active shielding, using a current-carrying loop driven in opposition to the stray field, is one approach that has been demonstrated in the literature [11] and would be the preferred solution if passive geometry changes proved insufficient.

One aspect of the design that the present results do not fully address is dynamic charging — transfer of power while the vehicle is moving, rather than parked. The LCC-S topology is well suited to this application because of its load-independent behaviour, but the DDQ receiver pad would need to be extended into a rail configuration, which is a different engineering problem. The authors regard this as a longer-term extension rather than a near-term priority.

VI. CONCLUSION

This paper has described an 11.2 kW wireless EV charger built around an LCC-S compensation topology, SiC switching at 85 kHz, and a DDQ receiver coil. The system achieves 93.4 % end-to-end efficiency at a 150 mm air gap, charges a 40 kWh battery from 10 % to 80 % SOC in 2.8 hours, tolerates lateral misalignment up to 100 mm while maintaining efficiency above 87 %, and complies with both ICNIRP EMF limits and CISPR 32 conducted/radiated emissions requirements.

Among published systems at comparable power levels, this represents the best reported combination of efficiency and misalignment tolerance.

The LCC-S topology's ability to maintain ZVS switching across a wide coupling range is probably the single most important factor in the efficiency result, and the case for adopting it over simpler SS or SP alternatives at power levels above 6 kW appears fairly strong on the basis of the data presented here. The DDQ receiver adds winding and assembly cost relative to a plain DD pad, but the misalignment tolerance benefit is substantial enough that it is difficult to justify the simpler option for a public charging context where parking accuracy cannot be controlled.

Future work will focus on three areas: closing the EMF compliance margin through active shielding, integrating vehicle positioning feedback to improve alignment before charging begins, and extending the system to 22 kW for rapid public charging applications where a larger transmitter pad and higher inverter current rating are needed.

ACKNOWLEDGEMENT

The authors thank the Power Electronics Laboratory at SGGS Institute of Engineering and Technology, Nanded, for access to the prototype assembly and testing facilities. Financial support from the DST-SERB Early Career Research Award (grant no. ECR/2024/001482) is gratefully acknowledged. The authors also thank Wolfspeed and EPC for providing engineering samples of the SiC and GaN devices used in the prototype.

REFERENCES

[1] S. Li and C. C. Mi, "Wireless power transfer for electric vehicle applications," IEEE Journal of Emerging and Selected Topics in Power Electronics, vol. 3, no. 1, pp. 4–17, 2015.

[2] C. S. Wang, O. H. Stielau, and G. A. Covic, "Design considerations for a contactless electric vehicle battery charger," IEEE Transactions on Industrial Electronics, vol. 52, no. 5, pp. 1308–1314, 2005.

[3] X. Qu, H. Han, S. C. Wong, C. K. Tse, and W. Chen, "Hybrid IPT topologies with constant current or constant voltage output for battery charging applications," IEEE Transactions on Power Electronics, vol. 30, no. 11, pp. 6329–6337, 2015.

[4] Z. Huang, S. C. Wong, and C. K. Tse, "Design of a single-stage inductive-power-transfer converter for efficient EV battery charging," IEEE Transactions on Vehicular Technology, vol. 66, no. 7, pp. 5808–5821, 2017.

[5] M. Budhia, G. Covic, and J. Boys, "Design and optimisation of circular magnetic structures for lumped inductive power transfer systems," IEEE Transactions on Power Electronics, vol. 26, no. 11, pp. 3096–3108, 2011.

[6] A. Zaheer, G. A. Covic, and D. Kacprzak, "A bipolar pad in a 10-kHz 300-W distributed IPT system for AGV applications," IEEE Transactions on Industrial Electronics, vol. 61, no. 7, pp. 3288–3301, 2014.

[7] W. Li, H. Zhao, J. Deng, S. Li, and C. C. Mi, "Comparison study on SS and double-sided LCC compensation topologies for EV/PHEV wireless chargers," IEEE Transactions on Vehicular Technology, vol. 65, no. 6, pp. 4429–4439, 2016.

[8] T. Tan, K. Kim, and H. Cho, "SiC-based 6.6 kW wireless EV charger with DD coil and LCC-S compensation," IEEE Access, vol. 11, pp. 24581–24592, 2023.

[9] J. L. Villa, J. Sallan, J. F. S. Osorio, and A. Llombart, "High-misalignment tolerant compensation topology for ICPT systems," IEEE Transactions on Industrial Electronics, vol. 59, no. 2, pp. 945–951, 2012.

[10] M. Budhia, J. T. Boys, G. A. Covic, and C. Y. Huang, "Development of a single-sided flux magnetic coupler for electric vehicle IPT charging systems," IEEE Transactions on Industrial Electronics, vol. 60, no. 1, pp. 318–328, 2013.

[11] S. Cruciani, T. Campi, F. Maradei, and M. Feliziani, "Active shielding design and optimization of a wireless power transfer (WPT) system for automotive," Energies, vol. 13, no. 18, art. 4575, 2020.